Asymptotic dispersion in 2D heterogeneous porous media determined by parallel numerical simulations

Jean-Raynald de Dreuzy, Anthony Beaudoin, Jocelyne Erhel

Asymptotic dispersion in 2D heterogeneous porous media determined by parallel numerical simulations

Jean-Raynald de Dreuzy[1], Anthony Beaudoin[2,3] and Jocelyne Erhel[2]

1- Géosciences Rennes (UMR CNRS 6118), Université de Rennes 1, 35042 Rennes cedex, France.

2- IRISA / INRIA of Rennes, Campus de Beaulieu, 35042 Rennes cedex, France.

3- Now at LMPG (Laboratoire de Mécanique, Physique et Géosciences), Université du Havre, 25 rue Philippe Lebon, BP 540, 76058 Le Havre cedex, France.

Abstract

We determine the asymptotic dispersion coefficients in 2D exponentially-correlated lognormally-distributed permeability fields by using parallel computing. Fluid flow is computed by solving the flow equation discretized on a regular grid and transport triggered by advection and diffusion is simulated by a particle tracker. To obtain a well-defined asymptotic regime under ergodic conditions (initial plume size much larger than the correlation length of the permeability field), the characteristic dimension of the simulated computational domains was of the order of 10^3 correlation lengths with a resolution of ten cells by correlation length. We determine numerically the asymptotic effective longitudinal and transverse dispersion coefficients over 100 simulations for a broad range of heterogeneities $\sigma^2 \in [0,9]$, where σ^2 is the lognormal permeability variance. For purely advective transport, the asymptotic longitudinal dispersion coefficient depends linearly on σ^2 for $\sigma^2<1$ and quadratically on σ^2 for $\sigma^2>1$ and the asymptotic transverse dispersion coefficient is zero. Addition of homogeneous

isotropic diffusion induces an increase of transverse dispersion and a decrease of longitudinal dispersion.

I. Introduction

The determination of the large-scale dispersion coefficients has been widely debated in the last twenty years [*Dagan*, 1989; *Gelhar*, 1993]. The classical case is the lognormal permeability field with an exponential correlation function such as:

$$C(r) = \sigma^2 \exp\left(-\frac{|r|}{\lambda}\right) \tag{1}$$

where σ^2 is the log-normal permeability variance, $|r|$ is the distance between two points and λ is the correlation length. Solute transport processes are advection and homogeneous isotropic diffusion. We look at the asymptotic dispersion coefficient for large heterogeneity corresponding to $\sigma^2 \in [1,9]$. Numerical simulations did not previously lead to definitive solutions because of the large times and equivalent domain dimensions required for the convergence to the asymptotic regime.

Two types of numerical simulations have been performed according to the derivation method of the velocity field. The velocity field is classically computed either directly from discretizing and solving the flow equation or from the first-order approximation of the flow equation. The computational domain is of dimensions L_x and L_y in the two spatial dimensions x and y. L_x and L_y are counted in terms of correlation length. The correlation length λ is counted in terms of grid cells. If we note l_m the dimension of the grid cell, the ratios L_x/λ, L_y/λ and λ/l_m should be as large as possible. Discretizing the flow equation yields a linear system of order proportional to the number of grid cells whatever the finite difference or finite element scheme [*Bellin, et al.*, 1992; *Cvetkovic, et al.*, 1996; *Hassan, et al.*, 2002; *Salandin*

and Fiorotto, 1998; *Trefry, et al.*, 2003] (Details of numerical simulations are given in Table 1). It explains why the direct solving of the flow equation has been limited to some 10^5 cells number. It corresponds to some tens of exploitable correlation lengths that turn out to be not enough for determining directly the asymptotic dispersion coefficient. Convergence to the asymptotic regime is slow requiring very large simulations [*Bellin, et al.*, 1992]. This study also shows a pronounced realization effect also obtained in [*Trefry, et al.*, 2003]. The realization effect consists first in large dispersion coefficient variations and secondly in deviations from the mean behavior. It has two implications. First, the second-order moment of the solute plume requires a large number of Monte-Carlo realizations and particles to achieve convergence. Secondly, it emphasizes the problem of the relevance of the mean behavior to natural cases which are inherently single realizations requiring conditioning on measurements and the use of an inverse problem methodology.

The other simulation method consists in deriving the velocity field from the first order approximation of the flow equation and performing subsequently a particle tracking [*Bellin, et al.*, 1992; *Dentz, et al.*, 2002; *Rubin*, 1990; *Schwarze, et al.*, 2001] (Table 1). This methodology does not require a grid and shortcuts the linear system solving step. Very long particle paths can be simulated and the asymptotic coefficients can be determined. In practice the average particle path length reached by this method is around hundred times larger than that obtained by the previous direct simulation method with a resolution five times finer (Table 1). However this methodology is limited to the validity domain of the first-order approximation ($\sigma^2<1$). For larger heterogeneities, deviations of the velocity field from the normal behavior are non negligible and increase with σ^2 [*Salandin and Fiorotto*, 1998]. The longitudinal velocity distribution becomes asymmetrical and is between the normal and lognormal distributions. The transverse velocity distribution becomes flatter with larger tails than that of the normal distribution. The first-order approximation of the velocity field does

not capture these effects. Moreover, the use of first-order approximated velocity field may lead to erroneous numerical results. In fact, for even not too large heterogeneity (σ^2=1), the first-order approximation produces closed streamlines in which particles can enter either by advection or by diffusion increasing artificially dispersion [*Dentz, et al.*, 2003].

Neither the direct solution nor the first-order approximation of the flow simulation have led to direct numerical estimates of the asymptotic transverse and longitudinal dispersion coefficients for broad heterogeneous permeability fields (σ^2>1). The only numerical estimate is provided by *Salandin and Fiorotto* [1998] and concerns the dependency of the asymptotic longitudinal dispersion coefficient D_{LA} on σ^2. They assume that the Lagrangian integral scale λ_{ux} is independent of σ^2 and estimate numerically the Lagrangian velocity variance $u_{\mathrm{xx}}(0)$. As $D_{LA} \approx \lambda_{ux} \cdot u_{xx}(0)$ in the asymptotic regime, they found $D_{LA} \propto \sigma^{\beta}$ with β=2.06, 2.19, 2.29 and 2.35 respectively for σ^2 in the intervals [0.05,1], [1,2], [2,3] and [3,4].

Analytical estimates of the dispersion coefficient come from first-order and second-order approximations of the flow and transport equations. First-order approximations yield a linear dependence of the asymptotic longitudinal dispersion coefficient D_{LA} on σ^2 and a zero asymptotic transverse dispersion coefficient D_{TA} for purely advected solutes [*Gelhar*, 1993]:

$$D_{LA} = u \cdot \lambda \cdot \sigma^2 \quad \text{and} \quad D_{TA} = 0 \tag{2}$$

where u is the mean velocity. Adding diffusion slightly reduces the asymptotic dispersion coefficient D_{LA} for isotropic diffusion and *Pe* larger than 10 [*Fiori*, 1996]. Second-order approximation of the transport equation has been taken into account and confirms the zero asymptotic transverse dispersion coefficient [*Hsu, et al.*, 1996]. For the longitudinal dispersion coefficient and values of σ^2 larger than 1 (σ^2=1.6 in [*Bellin, et al.*, 1992]), first-order approximations of the flow and transport equations remain very close to numerical

92 results [*Dagan, et al.*, 2003]. Adding a second-order term does not improve the approximation
93 of the longitudinal dispersion coefficient but on the contrary deteriorates it. It has thus been
94 deduced that the independent linearizations of flow and transport induce opposite deviations
95 from linear theoretical results that partly cancel out each other. These conclusions concerning
96 both the zero asymptotic transverse dispersion coefficient and the performance of the first-
97 order approximation were confirmed on slightly different heterogeneous media consisting in
98 spherical inclusions in a homogeneous medium [*Dagan, et al.*, 2003; *Jankovic, et al.*, 2003].
99 Other theoretical frameworks have been used to estimate the 2D asymptotic transverse
100 dispersion coefficient D_{TA}. Using volume averaging, D_{TA} is null like with the first-order
101 approximation [*Attinger, et al.*, 2004], whereas D_{TA} is not null by using the conjecture of
102 Corrsin [*Dentz, et al.*, 2002].

103 In this article, we compute the effective asymptotic longitudinal and transverse dispersion
104 coefficients for large heterogeneities ($\sigma^2 \in [0.25,9]$) both for pure advection and
105 homogeneous isotropic diffusion cases. To reach the asymptotic regime, we use very large
106 computational domains (100 times larger than the largest previously studied) under ergodic
107 conditions (large plume sizes compared to the correlation length of the permeability field).
108 We compare our results to the previous numerical results and analytical predictions.

109 II. Numerical methods

110 *II.1. Assumptions and notations*

111 We study 2D heterogeneous permeability field following a lognormal exponentially
112 correlated distribution as stated in the introduction (equation (1)). We perform the study on a
113 large range of σ^2 values ($\sigma^2 \in [0.25,9]$) first because broad-range heterogeneities have been
114 observed in the field (for example $\sigma^2 \sim 5$ for the Columbus site [*Rehfeldt, et al.*, 1992]) and

115 secondly to test theoretical predictions. Solutes are transported by advection and diffusion.
116 Diffusion is homogeneous with a diffusion coefficient noted *d*, the Peclet number *Pe*
117 expressing the ratio between advection and diffusion is equal to $Pe = (\lambda \cdot u)/d$, where *u* is
118 the mean velocity.

119 As seen in introduction, discretizing and solving the flow equation for obtaining the velocity
120 field computation is necessary for large heterogeneities (σ^2>1). From previous simulation
121 results obtained by using the first-order approximated velocity field (Table 1), the necessary
122 domain dimensions to asymptotic regime is around a thousand of correlation lengths with a
123 resolution of around 10 cells by correlation length [*Ababou, et al.*, 1989] leading to a number
124 of cells of the order of 10^8. Such large domains require parallel computing.

125 ### *II.2. Permeability field generation*

126 The software must be fully parallelized as the computational domain itself cannot be stored on
127 a unique processor. The computational domain is distributed from the beginning to the end of
128 the simulation, according to a domain decomposition in vertical slices (figure 1). Each
129 processor owns a well-defined part of the array corresponding to a sub-domain and keeps in
130 local memory one layer of cells surrounding its sub-domain. These cells called “ghost cells”
131 are necessary for the determination of the inter-cell permeability on sub-domain boundary
132 cells. The additional cost of memory use is negligible and the communication cost between
133 neighbouring processors is reduced.

134 The generation of the correlated lognormal field is performed via a Fourier transform
135 [*Gutjahr*, 1989]. We use the software FFTW [*Frigo and Johnson*, 2005]. This library has a
136 variety of composable solvers representing different FFT algorithms and implementation
137 strategies, whose combination into a particular plan for a given size can be determined at
138 runtime according to the characteristics of the machine/compiler in use. The construction of

the permeability field ends up with filling up the ghost cells, requiring the management of some communication between the processors. Permeability, velocity components and head values are all stored on the same types of array. The permeability field obtained from the Fourier transform methodology gives the right correlation length. The obtained variance is generally slightly smaller than the targeted variance [*Yao*, 2004]. More precisely, the variance is lowered by half the value of the mean. To avoid this bias we first generate a Gaussian correlated random field with zero mean and unitary variance. As we use a zero mean, the output variance is equal to the input targeted one. To obtain the right field, we first multiply the generated field by the standard deviation and add the logarithm of the geometric mean. We secondly take the exponential of the result. We calculated the obtained variance and found a value close at 0,02% to the input one for 8192^2 grids.

II.3. Flow computation

We discretize the classical flow equation $\nabla(K\nabla h)=0$ with K and h the permeability and hydraulic head and apply permeameter-like boundary conditions consisting in fixed head on two opposite borders and no flow on the perpendicular borders (figure 1). The flow equation is discretized according to a finite-difference scheme with harmonic inter-cell permeabilities. For regular square grids, this scheme is equivalent to mixed hybrid finite elements [*Chavent and Roberts*, 1991]. This equivalence ensures to these finite differences the high precision of the mixed hybrid finite elements useful for large permeability contrasts [*Mosé, et al.*, 1994]. The discrete flow equations end up to a linear system $Ax=b$, where A is a symmetric positive definite sparse structured matrix. The order of A is equal to the number of cells. The choice of the linear solver is essential to achieve the CPU and memory requirements for such large computational domains.

Several methods and solvers exist for these linear systems. They can be divided into three classes: direct, iterative and semi-iterative [*Meurant*, 1999; *Saad*, 1996]. Direct methods are highly efficient but require a large memory space. Iterative methods of Krylov type require less memory but need a scalable preconditioner to remain competitive. Iterative methods of multigrid type are often efficient and scalable, well-suited to regular grids, used by themselves or as pre-conditioners, but are sensitive to condition numbers [*Wesseling*, 2004]. The condition number is related to the heterogeneities considered and increases very rapidly with the variance. Semi-iterative methods such as subdomain methods are hybrid direct/iterative methods which can be good tradeoffs [*Toseli and Widlund*, 2005]. For iterative and semi-iterative methods, the convergence and the accuracy of the results depend on the condition number which can blow up at large scale for a high variance (σ^2>4). Because the memory space is more critical than the CPU time, we chose an iterative multigrid method. We used a numerical library HYPRE and more precisely Boomer-AMG (Algebraic MultiGrid) whose advantages are to be free, heavily used, portable and parallel [*Falgout, et al.*, 2005]. With this method, the CPU time is indeed not sensitive to the permeability variance. For a grid of 1.3 10^8 nodes with σ^2=6.25, the flow computation requires around half an hour on a cluster of a 32 bi-processor AMD Opteron 2.2 GHz with 2 Go RAM each interfaced by Gigabit Ethernet.

II.4. Transport simulation

Transport is simulated by a particle tracker algorithm [*Delay, et al.*, 2005]. Particle tracking is well suited for pure advection and advection-dominated transport processes because it does not introduce spurious numerical diffusion. Advection is simulated by a first order explicit scheme. We tried higher-order schemes which led to very small differences. Under this assumption of homogeneous isotropic diffusion, this method correctly models diffusion and

does not require any correction of the velocity term necessary for taking into account diffusion discontinuities [*Delay, et al.*, 2005]. Between t and t+dt, a particle moves from positions $M(t)$ to $M(t+dt)$ by advection and diffusion:

$$M(t+dt) = M(t) + v[M(t)] \cdot dt + \sqrt{2 \cdot d \cdot dt} \cdot Z \cdot r$$

where $v[M(t)]$ is the velocity at the position M, d is the diffusion coefficient, Z is a random number drawn from a Gaussian distribution of mean 0 and variance 1 and r is a unitary vector with uniformly distributed orientation. The time step evolves along the particle path according to the velocity magnitude of the crossed cells. More precisely, the time step is either proportional to the local advection time equal to the cell size l_{m} divided by the maximum of the velocities computed on the cell borders noted $v_{x+}, v_{x-}, v_{y+}, v_{y-}$ in the x and y directions or to the diffusion time necessary to cross the cell:

$$dt = \frac{1}{N_\alpha} \cdot \min\left[\frac{l_m}{\max\left(v_{x+}, v_{x-}, v_{y+}, v_{y-}\right)}, \frac{l_m^2}{2d} \right].$$

N_α is a positive integer representing the order of the time step number performed by the particle in the cell. In the simulations N_α is set to 10, meaning that the particle makes of the order of 10 steps to cross the cell. The velocity $v[M(t)]$ is obtained from a bilinear interpolation as it is the sole interpolation method that ensures mass conservation [*Pollock*, 1988]. It is important to find the exit position of the particle from the cell in order that particles always move in the cell with the velocity characteristics of the current cell and not of the previous one [*Pokrajac and Lazic*, 2002]. The exit point and time from the cell are found by linear interpolations. Diffusion is simulated by adding a random displacement of length proportional to the square root of time and of the diffusion coefficient [*Tompson and Gelhar*, 1990].

To avoid border effects, particles are introduced at a distance 0.05 L_x from the left border (input border) of the computational domain (figure 1) corresponding for L_x=8192 l_m and L_y=16384 l_m and λ=10 l_m (10 cells by correlation length) to respectively 40 and 80 correlation lengths downstream from the fixed head boundary. Particles are stopped when arriving at the same distance upstream from the right border (output border). For all simulations, the injection window is a thin line perpendicular to the mean flow direction of length equal to 3277 l_m (i.e. 0.4 L_y or around 328 correlation lengths for λ=10 l_m). Particles are injected with a uniform distribution within the injection window. The extension of the injection window is large enough to ensure a broad sampling of the velocity field but narrow enough to prevent particles from sampling the zones close to the no-flow boundary conditions [*Salandin and Fiorotto*, 1998]. The number of particles approaching the no-flow border of the domain by less than 15% of the domain dimension (120 correlation lengths) is recorded and found to be null. This "exclusion zone" close to the no-flow boundaries is shown on figure 1. The particle-tracking algorithm has been adapted for parallel simulations with the domain stored on the different processors [*Beaudoin, et al.*, 2007]. The time necessary for the simulation transport was at most equal to the time required for the computation of flow.

III. Dispersion computation, convergence and validation

Simulations give the first two moments of the particle plume distribution $< x(t) >_i$ and $< x^2(t) >_i$, here expressed in the longitudinal direction x:

$$< x^k(t) >_i = \frac{1}{N_p} \sum_{j=1}^{N_p} x_j(t)^k \qquad (3)$$

with *i* the simulation number, $x_j(t)$ the abscissa of the particle *j*, *k* the moment order (1 or 2), and N_p the number of particles. We compute a normalized dispersion coefficient by using the classical formula

$$D_L^i(t) = \frac{1}{u\lambda}\frac{1}{2}\frac{d\left(< x^2(t) >_i - < x(t) >_i^2\right)}{dt} \tag{4}$$

and discretize it on the successive time steps. The normalization factor $u\lambda$ is logical in terms of dimension to obtain a non-dimensional result. It is further justified for $\sigma^2<1$ by the first-order longitudinal dispersion coefficient linear in $u\lambda$ (equation 2). In the following, the term dispersion coefficient will refer to this normalized dispersion coefficient. We normalized the time *t* as well by the characteristic time λ/u needed for the flux to cross a correlation length and denote it $t_N = ut/\lambda$.

III.1. Asymptotic dispersion coefficient

We determine the asymptotic dispersion coefficient D_{LA}^i from the time derivative signal (4) according to the two following methods. Both methods rely on the late time behavior of the dispersion coefficient $D_L^i(t_N)$. The first method consists in averaging $D_L^i(t_N)$ over the time range $\left[0.5\,t_{fb}, t_{fb}\right[$ over which $D_L^i(t_N)$ is observed to have reached its asymptotic limit, where t_{fb} is the first breakthrough time (time for which the first particle arrives at a distance of $0.05L_x$ from the output border). The asymptotic dispersion coefficient is the average noted $D_{LA}^i(av)$. The second method is a simple fit of $D_L^i(t_N)$ over the whole time range by the exponential function

$$D_L^i(t_N) \approx D_{LA}^i(fit)\cdot\left(1-\exp\left(-t_N / t_{N0}^i\right)\right) \tag{5}$$

where $D_{LA}^{i}(fit)$ is the asymptotic dispersion coefficient. t_{N0}^{i} is a characteristic convergence time to the asymptotic regime. For the transverse dispersion coefficient, we derived the realization-based coefficient $D_T^i(t_N)$ by using the same methodology applying equations (3) and (4) where we replace *x* by *y*. Because of the absence of any systematic time evolution, we determine the asymptotic dispersion coefficient by averaging over the second part of the time range $\left[0.5\,t_{fb}, t_{fb}\right[$ like for the longitudinal dispersion coefficient. Whatever the method, the key point is to simulate transport in a sufficiently large domain to observe the stabilization of dispersion on a time range long enough. The relevance of the asymptotic dispersion coefficient depends on the domain dimensions counted in terms of correlation length L_x/λ and L_y/λ.

The mean and standard deviations of the dispersion coefficients as a function of time $D_L(t_N) = < D_L^i(t_N) >_{i=1..N_S}$ and $\sigma[D_L(t_N)] = \left[< D_L^i(t_N)^2 >_{i=1..N_s} - < D_L^i(t_N) >_{i=1..N_s}^2 \right]^{1/2}$ and the mean of the asymptotic dispersion coefficients $D_{LA} = < D_{LA}^i >_{i=1..N_S}$ are thereafter determined over N_S different realizations. The parameters controlling the determination of the asymptotic dispersion coefficients are the domain dimensions L_x/λ and L_y/λ, the number of particles N_p and the number of simulations N_S. First simulations have shown that domains should be of dimensions (L_x/λ, L_y/λ) equal to (820,820) and (1640,820) for respectively $\sigma^2 \le 4$ and $\sigma^2 \ge 6.25$ to have a long enough signal. We use these values to study the convergence with N_p and N_S and verify after that these dimensions are indeed large enough. We study successively the convergence as functions of the number of particles N_p and of the number of simulations N_S. Two averaging methods are possible leading respectively to the effective and ensemble dispersion coefficients. The effective dispersion is obtained by first computing the derivative of the standard deviation of the plume concentration within a simulation and

secondly by averaging the computed standard deviations over the N_S simulations. The ensemble dispersion is obtained by first computing the two first moments of the plume concentrations over the N_S simulations and by secondly computing the derivative of the standard deviation from the previous moments. The ensemble dispersion is larger than the effective dispersion as it measures the plume dispersion with respect to the plume position averaged over all simulations whereas the effective dispersion measures the plume dispersion in each simulation with respect to the simulation mean plume position [*Dentz, et al.*, 2000].

III.2. Convergence with the number of particles N_p

Figure 2 displays the dispersion coefficients $D_L^i(t_N)$ and $D_T^i(t_N)$ for number of particles N_p ranging from 100 to 10000. We choose an example in the most heterogeneous case (σ^2=9) without diffusion (pure advection). For N_p=100 (crosses), the dispersion coefficients are much more variable than for N_p=1000 (stars). Increasing the number of particles over 1000 does not change the global tendencies of the dispersion coefficients. Finally between 5000 and 10000, differences are very small. At a given time, the dispersion coefficient can be well approached with N_p=10000 particles. We computed also the asymptotic dispersion coefficients $D_{LA}^i(av)$ and $D_{TA}^i(av)$ according to the number of particles N_p in the most heterogeneous cases (σ^2=6.25 and 9) for Peclet numbers *Pe* ranging from 100 to ∞. *Pe*=∞ corresponds to the pure advection case (without diffusion) (figure 3). For $N_p \geq 2000$, $D_{LA}^i(av)$ and $D_{TA}^i(av)$ do not vary much with the number of particles. More precisely, they vary respectively by less than 5% and 10% whatever the case. There is no systematic tendency either with the number of particles or with the Peclet number. We kept for the pure-advection case 10000 particles and for the advection-diffusion case 2000 particles. As convergence is not faster without diffusion as shown by figure 3, this choice does not advantage the pure advection case more than the

294 5% and 10% precisions previously found. The global number of particles can be converted
295 into number of particles by correlation length at injection time. For all cases the injection
296 window was set to 3277 l_m. For the pure-advection case N_p=10000, the number of particles by
297 cell is 3 on average and the number of particles by correlation length is 30 on average because
298 there are 10 cells by correlation length (λ=10 l_m). For the advection-diffusion case N_p=2000,
299 the number of particles by cell is 0.6 on average and with λ=10 l_m, the number of particles by
300 correlation length is 6 on average.

301 ### *III.3. Convergence with the number of simulations N_S*

302 We study the convergence of the average and standard deviation of the dispersion coefficients
303 with the number of simulations N_S for the most heterogeneous cases σ^2=6.25 and 9. The mean
304 longitudinal asymptotic dispersion coefficient is very close to the mean of the dispersion
305 coefficient taken at a given time t_N=600 (figure 4a, solid and open squares compared to thick
306 solid and dashed grey lines). The asymptotic dispersion coefficient converges very rapidly for
307 $N_S \geq 20$. The largest difference between values for 20 and 100 simulations is of the order of
308 2.5%. The standard deviation of the longitudinal dispersion coefficient at the same given time
309 t_N=600 $\sigma\left(D_L\left(t_N = 600\right)\right)$ displays relative larger variations with the number of simulations N_S
310 (figure 4b, lines and symbols). The maximal variation between N_S=20 and N_S=100 is 20%. As
311 variations are not monotonous, the value for the largest number of simulations cannot be more
312 precise than 20%. We note that both the variability of the average asymptotic dispersion
313 coefficients and the standard deviation of the dispersion coefficient decrease with more
314 diffusion (smaller Peclet numbers). Convergence of the longitudinal dispersion coefficient
315 with the number of simulations is thus faster with more diffusion.

316 Tendencies for the transverse dispersion coefficient are quite different. For $N_S \geq 20$, the
317 asymptotic dispersion coefficient is very close to zero for the pure-advection case (figure 5a)
318 whereas the standard deviation of the transverse dispersion coefficient at a given time is much
319 larger around 0.6 (figure 5b). More diffusion corresponding to smaller Peclect numbers
320 induces larger transverse asymptotic dispersion and standard deviation. The asymptotic
321 transverse dispersion coefficient (figure 5a) converges quickly and its variations for $N_S \geq 20$
322 are less than 10% of its mean value. The standard deviation (figure 5b) still varies non
323 monotonously and the amplitude of its variations can reach 25% of its mean value.

324 In the two previous sections, we have fixed the mesh size l_m and analyzed the convergence of
325 the random walker and the Monte-Carlo simulations. For a given simulation, we verified
326 numerically that the random walker converges when we increase the number of particles.
327 More precisely, the dispersion coefficients $D_L(t)$ and $D_T(t)$ converge. We can assume a
328 convergence in an appropriate norm; in view of the numerical results, we can also assume a
329 uniform convergence, independent of the simulations. For a given number of particles, we
330 verified numerically that the Monte-Carlo simulations converge when we increase the number
331 of simulations. More precisely, we observe the convergence of the approximate first moments
332 of the dispersion, computed with a given number of particles. Therefore, we can assume that,
333 for a given mesh size l_m, our numerical Monte-Carlo simulations give an accurate estimation
334 of the first moments of the two dispersion functions. However, in our simulations, the second
335 moments do not converge correctly. There may be different reasons for this lack convergence.
336 First the number of Monte-Carlo simulations N_S may not be large enough. Secondly
337 dispersion coefficient may be affected by the finite volume method used for flow computation
338 and the use of a bilinear interpolation for the velocity in the particle tracker. Thirdly, it may
339 come from the generation of the permeability field from a truncated Fourier expansion and the
340 assumption of a constant permeability in each grid cell. The same lack of convergence of the

dispersion fluctuations has already been observed and related to the finite number of Fourier modes (figure 5 of [*Eberhard*, 2004]).

In the following, we perform 100 simulations to ensure convergence of the first moments D_{LA} and D_{TA} for each parameter set. We keep the same parameters for all simulations. As the variations of both the longitudinal and transverse dispersion coefficients are stronger for σ^2=9 than for σ^2=6.25, we checked that convergence is at least as good for lower heterogeneities corresponding to $\sigma^2 \leq 6.25$.

III.4. Convergence of dispersion coefficients with time

The domain dimensions were chosen in order to have a stabilization of the mean dispersion coefficient as a function time $D_L(t_N)$ over at least half the time duration of the simulation, the maximal simulation time t_{fb} being the first breakthrough time (time for which the first particle arrives at a distance of $0.05L_x$ from the output border). The asymptotic regime is maintained over around 500 time units or equivalently on a spatial range of 500 correlation lengths. The simulations performed on domain of longitudinal dimension L_x=819,2 λ with λ=10 l_m were large enough for $\sigma^2 \leq 4$. For σ^2=1, the asymptotic regime is reached after some tens of correlation lengths (figure 6a). However for $\sigma^2 \geq 6.25$, domains had to be twice longer (L_x=1638,4 λ) to obtain the same stabilization time range (figure 6b). Such long stabilization times have also been observed in systems made of highly heterogeneous inclusions [*Jankovic, et al.*, 2006]. Large domain dimensions are required not only for large values of σ^2 but also for smaller values of σ^2 (values around 1), although it is not obvious on figure 6a. In fact we performed the same simulations for domains of dimensions L_x=102,4 λ by L_y=51,2 λ and found that the asymptotic regime is far from being reached although the number of exploitable correlation lengths (~80) is large enough. There may be two reasons.

First the asymptotic regime is difficult to identify over some tens of correlation lengths. Secondly, the injection window is smaller (20 correlation lengths at L_y=512 l_m compared to 327 at L_y=8192 l_m) inducing from the beginning a lower sampling of the velocity field and a larger convergence time to the asymptotic regime.

The mean $D_L(t_N)$ and the confidence interval at 95% derived from the mean and standard deviation are represented on figure 6 (solid and dashed lines). $D_L^i(t_N)$ displays a large variability but no definite trend whatever σ^2 as shown by figure 6 (square and circle symbols). The average $D_L(t_N)$ of the dispersion coefficient over 100 simulations represented by the black line smoothens the variations and indeed reaches a constant value at small times (t_N>30) for σ^2=1 (figure 6a) and at larger times (t_N>400) for σ^2=9 (figure 6b). The asymptotic regime is well approached at least during the second half of the simulation time, i.e. in the interval $\left[0.5\,t_{fb}, t_{fb}\right[$. The realization-based $D_T^i(t)$ displays a strong variability around 0 but no trend, not even at small times (square and circle points on figure 7). The average over simulations (solid line of figure 7) does neither show any trend whereas the standard deviation (dashed lines of figure 7) is large compared to the average values.

We note that several studies have used the apparent dispersion coefficient $D_{app}(t) = 0.5 < x^2(t) > / t$ instead of the derivative (4) to remove the oscillations of the time derivative [*Schwarze, et al.*, 2001; *Trefry, et al.*, 2003]. Even though D_{app} tends to the effective dispersion coefficient (4) for large times, the differences between these two quantities are important and remain for very large times especially in the high variance case as shown by figure 6 on the simulation averages (dashed-dotted lines compared to solid lines). We thus decide to determine the asymptotic dispersion coefficient D_{LA}^i from the time derivative signal (4).

III.5. Validation

We validate the numerical procedures by comparing them to theoretical and other numerical existing results. First, for $\sigma^2<1$, we compare numerical results to first-order theoretical results of the correlation functions of the longitudinal and transverse velocity fields (equations 9 and 10 of [*Rubin*, 1990]) and of the asymptotic dispersion coefficients. The velocity correlation function is highly close at less than 5% to the first-order prediction for $\sigma^2<1$ and is close at less than 1.5% to the results of *Salandin and Fiorotto* [1998] for $1<\sigma^2<4$ (figure 8).

For the asymptotic longitudinal dispersion coefficient, the normalization by λu enables a direct comparison of D_{LA} numerical results with σ^2 for $\sigma^2<1$ with equation (2). The agreement is very good as, for $\sigma^2=0.25$, equation (2) and numerical simulations give respectively 0.25 and 0.26. We compare also our results of longitudinal asymptotic dispersion coefficient in the interval $1<\sigma^2<4$ to the variation of D_{LA} with σ obtained by *Salandin and Fiorotto* [1998]. *Salandin and Fiorotto* [1998] found $D_L \propto \sigma^{\beta}$ with β=2.06, 2.19, 2.29 and 2.35 respectively for σ^2 in the intervals [0.05,1], [1,2], [2,3] and [3,4]. We find β=2.07, 2.37 and 2.62 for σ^2 in the intervals [0.05,1], [1,2.25], and [2.25,4]. We find a close agreement in the first interval but a faster increase of the asymptotic dispersion coefficient for $\sigma^2>1$. This could be linked to the number of correlation lengths limited to 20 in *Salandin and Fiorotto* [1998]. For advective-diffusive transport, we validate the algorithm against the classical analytical solution obtained in the homogeneous medium case.

IV. Results of asymptotic dispersion coefficients

IV.1. Pure advection (Pe=∞)

We determine the effect of the resolution scale defined by the number of cells by correlation length λ/l_m. We perform the simulations at λ/l_m =5, 10 and 20 where previous simulations used a maximum of 8 cells per correlation length (Table 1). We verify that the asymptotic longitudinal dispersion coefficient depends linearly on λ for all values of σ^2 (figure 9) justifying furthermore the normalization of the dispersion coefficients by λu. It also shows the weak dependency of the asymptotic dispersion coefficient on the resolution of the discretization even for high heterogeneities. 10 cells by correlation length give very similar results as 5 or 20 cells by correlation length.

The asymptotic regime has been reached and maintained over at least 500 correlation lengths whatever the value of σ^2 (figure 10) and the asymptotic values of the dispersion coefficients have been computed according to the procedure described in the previous section (figure 11). Both methodologies of exponential fitting and averaging lead to similar results within an interval of 0% to 3%. The first-order estimate of the dispersion coefficient (2) remains close to the numerical value even for σ^2=1 and 2.25 where it is lower by respectively 10% and 25%. This good performance of first-order results for values of σ^2 significantly larger than 1 has been previously observed and explained [*Bellin, et al.*, 1992; *Dagan, et al.*, 2003]. The independent linearizations of flow and transport induce opposite deviations from linear theoretical results and may partly cancel out each other. This conclusion was confirmed on slightly different heterogeneous media consisting of spherical inclusions in a homogeneous medium [*Dagan, et al.*, 2003]. For larger heterogeneity, the departure from the first-order results increases with σ^2. Numerical results are respectively 50%, 90% and 150% larger than

the linear estimates for σ^2=4, 6.25 and 9. $D_{LA}(av)$ is well represented by the approximate function $0.7\,\sigma^2 + 0.2\,\sigma^4$ for large heterogeneities (σ^2>1) (dashed curve on figure 11).

For transverse dispersivity, numerical results show some variability around 0 without any systematic trend neither for the realization-based result nor for the average (figures 7 and 12). The similar transverse dispersion evolution with time for σ^2=6.25 and 9 comes from the fact that realizations are performed with the same set of seeds for the random generator. The correlation patterns are thus identical while the magnitude of the heterogeneity changes. The asymptotic dispersion coefficients computed by averaging over the second half of the time chronicle $D_{TA}(av)$ are close to zero without being systematically positive or negative (figure 13) and the magnitude of the standard deviation is much larger than the average. These results lead us to conclude that the asymptotic transverse dispersion coefficient is zero on average whatever σ^2. This confirms theoretical conclusions obtained by volume averaging [*Attinger, et al.*, 2004].

Figures 6 and 7 show a large variability around the average both for the longitudinal and transverse dispersion coefficients whatever the heterogeneity represented by the value of σ^2. The standard deviation of the transverse dispersion coefficient converges (figure 14b) within the computation time, whereas the convergence is not obvious for the standard deviation of the longitudinal dispersion coefficient (figure 14a). The apparent increase of the longitudinal dispersion coefficient remains limited to at most 30% in the time interval $[t_{fb}/2, t_{fb}]$, which is close to the imprecision of 20% obtained in section III.3 because of the use of a limited number of simulations (N_S). Convergence would require both more realizations and longer systems. As the increase remains limited and as $\sigma\left(D_L\left(t_N\right)\right)$ is not the main objective of the study, we did not go further on its characterization.

Finally, we derive from the exponential fit of the longitudinal dispersion coefficient the characteristic convergence time to the asymptotic regime t_{N0} (figure 15). t_{N0} does not have an absolute meaning as it depends on the width of the injection window. We rather use t_{N0} to compare convergence time between different values of σ^2 in the same conditions. t_{N0} increases exponentially with the permeability variance contrarily to the first-order theory prediction according to which t_{N0} does not depend on the medium heterogeneity σ^2.

IV.2. Advection and diffusion (Pe<∞)

We computed the dispersion coefficient $D_L(t_N)$ for the two Peclet number *Pe*=100 and 1000. $D_L(t)$ reaches its asymptotic regime whatever the value of σ^2 (figure 16). The time to reach the asymptotic dispersion t_{N0} is smaller than in the pure-advection regime (figure 15) even if t_{N0} values are highly dispersed. Diffusion modifies only slightly the asymptotic longitudinal dispersion coefficient D_{LA} for $\sigma^2 \leq 1$ and let it decrease for $\sigma^2>1$ (Table 2). For small values of σ^2 ($\sigma^2 \leq 1$), the influence of diffusion is negligible as previously found [*Fiori*, 1996]. For $\sigma^2=1$, the additional dispersion induced by diffusion is not significant because the asymptotic dispersion coefficient for *Pe*=∞ (larger than 1) is ten times larger than 1/*Pe*. For $\sigma^2 > 1$, the asymptotic dispersion coefficient decreases surprisingly with more diffusion. More diffusion induces less dispersion. The decrease can be significant. For $\sigma^2=6.25$, D_{LA} is 25% lower at *Pe*=100 than its value at *Pe*=∞ (pure advection). For large heterogeneities, diffusion reduces the global dispersion. This behavior was expected by *Gelhar* [1993] (pages 221-222) and *de Arcangelis et al.* [1986] and may be explained by the following argument also invoked for percolation systems [*Koplik, et al.*, 1988]. Large dispersion is induced by the widely-scattered velocity distribution. Diffusion introduces a cut-off to this distribution thus narrowing it and letting in turn the dispersion coefficient decrease. In other words, diffusion extracts particles from the very slow velocity zones and restricts the dispersion of particle in the medium. The

transverse asymptotic dispersion coefficient D_{TA} keeps a more classical behavior by increasing with more diffusion (Table 2). However the increase of D_{TA} can be much larger than the sole diffusion contribution $1/Pe$. For large heterogeneities σ^2=6.25 and for Pe=100, D_{TA} is 20 times larger than $1/Pe$. The effect of diffusion and advection cannot be simply superposed but interact to produce a larger transverse dispersion.

V. Conclusion

We determine the asymptotic dispersion coefficients for 2D exponentially correlated lognormal permeability fields on a broad range of lognormal permeability variance σ^2 ($\sigma^2 \in [0.25,9]$). We use parallel computing for simulating fluid flow and particle transport on large domains of typical dimension from 800 to 1600 correlation lengths with a resolution of 10 cells by correlation length, where l_m is the cell characteristic dimension. Such large domains turned out to be necessary to observe the asymptotic regime on a sufficiently long time range for determining unambiguously the asymptotic dispersion coefficients. The asymptotic longitudinal and transverse dispersion coefficient D_{LA} and D_{TA} have been estimated on a realization basis by averaging over a traveled distance of at least 400 correlation lengths. We have tested an alternative derivation methodology for the asymptotic longitudinal dispersion coefficient D_{LA} by fitting the dispersion coefficient by an exponential function. Estimates of D_{LA} by both methodologies lead to very similar values. The characteristic time given by the exponential fit gives an estimate of the convergence speed to the asymptotic regime. Simulations show that it increases exponentially with the heterogeneity σ^2 and decreases with diffusion.

For pure advection (Pe=∞), the asymptotic longitudinal dispersion D_{LA} is larger than the first-order estimate for high heterogeneity. More precisely, for σ^2 equal to 4, 6.25 and 9, D_{LA} is larger by respectively 50%, 90% and 150% than the linear estimates. For σ^2>1, D_{LA} is well

500 fitted by the function $0.7\sigma^2 + 0.2\sigma^4$ showing a quadratic evolution in σ^2 for large
501 heterogeneities. This departure from the first-order theory is probably related to the extreme
502 flow channeling observed for high heterogeneity [*Le Borgne, et al.*, submitted; *Moreno and*
503 *Tsang*, 1994; *Salandin and Fiorotto*, 1998]. Whatever the heterogeneity level, the asymptotic
504 transverse dispersion coefficient is always zero as predicted by first-order theory for low
505 heterogeneity and by volume averaging [*Attinger, et al.*, 2004].

506 The addition of diffusion to advection leads to two very different behaviors for longitudinal
507 and transverse dispersions. For large heterogeneities (σ^2>1), diffusion induces a significant
508 longitudinal dispersion decrease and a transverse dispersion increase larger than expected. At
509 most, for a Peclet number of 100 (advection on average hundred times larger than diffusion)
510 and a permeability variance σ^2=9, the longitudinal dispersion decreases by a factor of 2 and
511 the transverse dispersion is 7.5 times larger than the local diffusion.

512

513 **Acknowledgements**: This work was supported by Grid'5000 grants for executing simulations
514 on the grid at Irisa in Rennes. Comments by referees and an editor have helped
515 improve the revised version of the paper.

516 ## References

517 Ababou, R., D. Mclaughlin, L. W. Gelhar, and A. F. B. Tompson (1989), Numerical
518 simulation of three-dimensional saturated flow in randomly heterogeneous porous
519 media, *Transport in Porous Media*.

520 Attinger, S., M. Dentz, and W. Kinzelbach (2004), Exact transverse macro dispersion
521 coefficients for transport in heterogeneous porous media, *Stochastic Environmental*
522 *Research and Risk Assessment*.

523 Beaudoin, A., J. R. de Dreuzy, and J. Erhel (2007), An efficient parallel tracker for advection-
524 diffusion simulations in heterogeneous porous media, paper presented at Europar,
525 Rennes, France, 28-31 August 2007.

526 Bellin, A., P. Salandin, and A. Rinaldo (1992), Simulation of dispersion in heterogeneous
527 porous formations: statistics, first-order theories, convergence of computations, *Water*
528 *Resources Research*, *28*, 2211-2227.

529 Chavent, G., and J. E. Roberts (1991), A unified physical presentation of mixed, mixed-
530 hybrid finite elements and standard finite difference approximations for the
531 determination of velocities in waterflow problems, *Advances in Water Resources*, *14*,
532 329-348.

533 Cvetkovic, V., H. Cheng, and X.-H. Wen (1996), Analysis of nonlinear effects on tracer
534 migration in heterogeneous aquifers using Lagrangian travel time statistics, *Water*
535 *Resources Research*, *32*, 1671-1680.

536 Dagan, G. (1989), *Flow and Transport in Porous Formations*, 465 pp., Springer Verlag.

537 Dagan, G., A. Fiori, and I. Jankovic (2003), Flow and transport in highly heterogeneous
538 formations: 1. Conceptual framework and validity of first-order approximations, *Water*
539 *Resources Research*, *9*.

540 de Arcangelis, L., J. Koplik, S. Redner, and D. Wilkinson (1986), Hydrodynamic Dispersion
541 in Network Models of Porous Media, *Physical Review Letters*, *57*, 996-999.

542 Delay, F., P. Ackerer, and C. Danquigny (2005), Solution of solute transport in porous or
543 fractured formations by random walk particle tracking: a review, *Vadose Zone Journal*,
544 *4*, 360-379.

545 Dentz, M., H. Kinzelbach, S. Attinger, and W. Kinzelbach (2000), Temporal behavior of a
546 solute cloud in a heterogeneous porous medium, 1, Point-like injection, *Water*
547 *Resources Research*, *36*.

548 Dentz, M., H. Kinzelbach, S. Attinger, and W. Kinzelbach (2002), Temporal behavior of a
549 solute cloud in a heterogeneous porous medium: 3. Numerical simulations, *Water*
550 *Resources Research*, *7*.

551 Dentz, M., H. Kinzelbach, S. Attinger, and W. Kinzelbach (2003), Numerical studies of the
552 transport behavior of a passive solute in a two-dimensional incompressible random flow
553 field, *Physical Review E*, *67*.

554 Eberhard, J. (2004), Approximations for transport parameters and self-averaging properties
555 for point-like injections in heterogeneous media, *Journal of Physics a-Mathematical*
556 *and General*, *37*, 2549-2571.

557 Falgout, R. D., J. E. Jones, and U. M. Yang (2005), Pursuing scalability for HYPRE's
558 conceptual interfaces, *ACM Transactions on mathematical software*, *31*.

559 Fiori, A. (1996), Finite Peclet extensions of Dagan's solutions to transport in anisotropic
560 heterogeneous formations, *Water Resources Research*, *32*, 193-198.

561 Frigo, M., and S. G. Johnson (2005), The Design and Implementation of FFTW3,
562 *Proceedings of the IEEE*, *93*, 216-231.

563 Gelhar, L. W. (1993), *Stochastic Subsurface Hydrology*, Engelwood Cliffs, New Jersey.

564 Gutjahr, A. L. (1989), Fast Fourier transforms for random field generation *(ed.)*, New Mexico
565 Tech project report 4-R58-2690R.

566 Hassan, A. E., R. Andricevic, and V. Cvetkovic (2002), Evaluation of analytical solute
567 discharge moments using numerical modeling in absolute and relative dispersion
568 frameworks, *Water Resources Research*, *38*.

569 Hsu, K. C., D. Zhang, and S. P. Neuman (1996), Higher-order effects on flow and transport in
570 randomly heterogeneous porous media, *Water Resources Research*, *32*, 571-582.

571 Jankovic, I., A. Fiori, and G. Dagan (2003), Flow and transport in highly heterogeneous
572 formations: 3. Numerical simulations and comparison with theoretical results, *Water*
573 *Resources Research*, *9*.

574 Jankovic, I., A. Fiori, and G. Dagan (2006), Modeling flow and transport in highly
575 heterogeneous three-dimensional aquifers: Ergodicity, Gaussianity, and anomalous
576 behavior - 1. Conceptual issues and numerical simulations, *Water Resources Research*,
577 *42*.

578 Koplik, J., S. Redner, and D. Wilkinson (1988), Transport and Dispersion in Random
579 Networks With Percolation Disorder, *Physical Review a*, *37*.

580 Le Borgne, T., J.-R. d. Dreuzy, P. Davy, and O. Bour (submitted), Characterization of the
581 velocity field organization in heterogeneous media by conditional correlations, *Water*
582 *Reosurces Research*.

583 Meurant, G. (1999), *Computer solution of large linear systems*, North Holland, Amsterdam.

584 Moreno, L., and C.-F. Tsang (1994), Flow channeling in strongly heterogeneous porous
585 media: A numerical study, *Water Resources Research*, *30*, 1421-1430.

586 Mosé, R., P. Siegel, and P. Ackerer (1994), Application of the mixed hybrid finite element
587 approximation in a groundwater model: Luxury or necessity?, *Water Resources*
588 *Research*, *30*, 3001-3012.

589 Pokrajac, D., and R. Lazic (2002), An efficient algorithm for high accuracy particle tracking
590 in finite elements, *Advances in Water Resources*, *25*, 353-369.

591 Pollock, D. W. (1988), Semianalytical computation of path lines for finite-difference models,
592 *Ground Water*, *26*, 743-750.

593 Rehfeldt, K. R., J. M. Boggs, and L. W. Gelhar (1992), Field study of dispersion in a
594 heterogeneous aquifer, 3, geostatistical analysis of hydraulic conductivity, *Water*
595 *Resources Research*, *28*.

596 Rubin, Y. (1990), Stochastic modeling of macrodispersion in heterogeneous porous media,
597 *Water Resources Research*, *26*, 133-141.

598 Saad, Y. (1996), *Iterative Methods for Sparse Linear Systems*, PWS Publishing Company.

599 Salandin, P., and V. Fiorotto (1998), Solute transport in highly heterogeneous aquifers, *Water*
600 *Resources Research*, *34*, 949-961.

601 Schwarze, H., U. Jaekel, and H. Vereecken (2001), Estimation of Macrodispersion by
602 Different Approximation Methods for Flow and Transport in Randomly Heterogeneous
603 Media, *Transport in Porous Media*, *43*, 265-287.

604 Tompson, A. F. B., and L. W. Gelhar (1990), Numerical simulation of solute transport in
605 three-dimensional, randomly heterogeneous porous media, *Water Resources Research*,
606 *26*, 2541-2562.

607 Toseli, A., and O. Widlund (2005), *Domain decomposition methods-algorithms and theory*,
608 springer series in computational mathematics.

609 Trefry, M. G., F. P. Ruan, and D. McLaughlin (2003), Numerical simulations of
610 preasymptotic transport in heterogeneous porous media: Departures from the Gaussian
611 limit, *Water Resources Research*, *39*.

612 Wesseling, P. (2004), *An Introduction to Multigrid Methods*, Edwards.

613 Yao, T. (2004), Reproduction of the Mean, Variance, and Variogram Model in Spectral
614 Simulation, *Mathematical Geology*, *36*, 487-506.

615

Figure captions

Figure 1: Permeability field stored on four processors, boundary conditions, injection and exclusion zones. The characteristics of the computational domain are $L_x=2048.l_m=204,8.\lambda$, $L_y=1024.l_m=102,4.\lambda$, $\lambda=10.l_m$ and $\sigma^2=2.25$ where λ is the correlation length and l_m is the grid cell size. Permeability is increasing from blue to red. Computational domains used for asymptotic dispersion determination where 4 to 8 times longer and larger than this one.

Figure 2: a) Longitudinal and b) transverse dispersion coefficients as functions of time for increasing particle numbers with $\sigma^2=9$, $\lambda=10\ l_m$ and $L_x=819,2.\lambda$ and $L_y=819,2.\lambda$ (pure advection case).

Figure 3: Asymptotic longitudinal (a) and transverse (b) dispersion coefficients as functions of the particle number N_p for $L_x=1638,4\ \lambda$ and $L_y=819,2\ \lambda$. In this figure as well as in the following figures, the term advection in the legend refers to the pure advection case without diffusion and the legend is the same for both graphs.

Figure 4: a) Asymptotic longitudinal dispersion coefficient and b) standard deviation of the dispersion coefficient at a given time $t_N=600$ as functions of the number of simulations for $L_x=1638,4\ \lambda$ and $L_y=819,2\ \lambda$. In a), the dispersion coefficient D_L for $t_N=600$ has been added for the pure advection cases. $t_N=600$ is taken in the second half of the signal as the full signal length is around $t_N=1000$.

Figure 5: a) Asymptotic transverse dispersion coefficient and b) standard deviation of the dispersion coefficient at a given time $t_N=600$ as functions of the number of simulations. Same parameters as in figure 6.

Figure 6: Normalized longitudinal dispersion coefficient for single realizations $D_L^i(t_N)$ *(points), their averages* $D_L(t_N)$ *over 100 realizations (lines) and the confidence interval at 95% on the dispersion coefficient (dashed line) (*σ^2*=1 and 9, pure advection case). The dashed-dotted* line *represents the normalized apparent dispersion coefficient* $D_{app}(t) = 0.5 < x^2(t) > / t$*. Computational domain size are for* σ^2*=1 (a)* L_x*=*L_y*=819,2* λ *and for* σ^2*=9 (b)* L_x*=1638,4* λ *and* L_y*=819,2* λ*.*

Figure 7: Normalized transverse dispersion coefficient. Same parameters as in figure 6.

Figure 8: Velocity variance u_{xx} *and* u_{yy} *as functions of* σ^2 *obtained analytically in Rubin [1990] and numerically in the present study and in Salandin and Fiorotto [1998].*

Figure 9: Asymptotic longitudinal dispersion coefficient as a function of the correlation length for the pure advection case. Lines are linear fit through 0. Same parameters as in figure 6.

Figure 10: Longitudinal mean dispersion coefficient as a function of t_N *for the pure advection case (time in terms of correlation scales crossed by the plume). Dashed lines mark the asymptotic coefficients. Same parameters as in figure 6.*

Figure 11: Normalized longitudinal asymptotic effective dispersion coefficient D_{LA} *as a function of the variance of the log conductivity with pure advection. Vertical bars on data points represent the standard deviation on each side of the data point.* D_{LA}*(av) and* D_{LA}*(fit) are obtained respectively by averaging and fitting by an exponential function. Theoretical predictions [Gelhar, 1993] are represented by the line. The dashed curve stands for* $0.7\sigma^2 + 0.2\,\sigma^4$*. Same parameters as in figure 6.*

Figure 12: Normalized transverse dispersion coefficient as a function of the normalized time in the pure advection case. Same parameters as in figure 6.

Figure 13: Normalized transverse asymptotic dispersion coefficient for the pure advection case.

Figure 14: Standard deviation of a) the longitudinal and b) transverse dispersion coefficients in the pure advection case.

Figure 15: Characteristic convergence time to the asymptotic regime t_{N0}.

Figure 16: Longitudinal dispersion coefficient as a function of normalized time for $\sigma^2 \geq 4$.

	FCM	TP	TCM	σ^2	λ/l_m	L_x/l_m	L_y/l_m	N_m	MC	PT
[*Rubin*, 1990]	1st	A	PT	0.79						300
[*Bellin, et al.*, 1992]	full	A	PT	$[0,1.6]$	8	36	18	$4\ 10^4$	MC · PT = 1500	
[*Cvetkovic, et al.*, 1996]	full	A	PT	$[0,4]$	4	24	18	$7\ 10^3$	500-1000	1
[*Salandin and Fiorotto*, 1998]	full	A	PT	$[0.05,4]$	2,4,8	64	64	$2.6\ 10^5$	500	40
[*Schwarze, et al.*, 2001]	1st	AD	PT	$[0.1,1]$	50	5000			3200	1
[*Hassan, et al.*, 2002]	full	A	PT	$[0.25,2.25]$	5	50	25	$3\ 10^4$	2000-3000	
[*Dentz, et al.*, 2002]	1st	AD	PT	$[0.1,2]$	20	1500			2000	100
[*Trefry, et al.*, 2003]	full	Aα	NS	$[0.25,4]$	8 2	256-1024	64-256	10^6	1	
this study	full	AD	PT	$[0.25,8]$	10	819-1638	819	$7\ 10^7$- $1.4\ 10^8$	100	2000

Table 1: Characteristics of 2D flow and transport simulations. FCM stands for flow computation method. It can be 1st order when flow is obtained by first order approximation of the flow equation or full when flow is obtained by solving directly the full discretized flow equation. TP is the transport processes accounted for (A for advection, D for diffusion, α for dispersion). TCM stands for transport computation method (PT for particle tracking, NS for numerical scheme). N_x and N_y are the number of correlation lengths within the domain respectively in the main direction of flow and perpendicularly to it. N_m is the total number of cells ($N_m = L_x L_y / l_m^2$). MC realizations is the number of Monte-Carlo realizations per parameter set. PT trajectories is the total number of analyzed trajectories per realization when particle tracking is used.

	$D_{LA}(Pe)/D_{LA}(advection)$		$D_{TA}(Pe)$	
	$Pe=10^2$	$Pe=10^3$	$Pe=10^2$	$Pe=10^3$
$\sigma^2=0.25$	1.08	1.06	0.01	0.00
$\sigma^2=1$	1.05	1.06	0.00	-0.01
$\sigma^2=2.25$	0.98	1.01	-0.06	0.05
$\sigma^2=4$	0.90	1.01	-0.06	-0.09
$\sigma^2=6.25$	0.75	0.96	0.20	0.14
$\sigma^2=9$	0.57	0.84	0.24	0.16

Table 2: Asymptotic longitudinal dispersion coefficient normalized by its pure advective counterpart $D_{LA}(Pe)/D_{LA}(advection)$ and asymptotic transversal dispersion coefficient as functions of σ^2 and Pe. Dispersion coefficients are obtained with the averaging method.

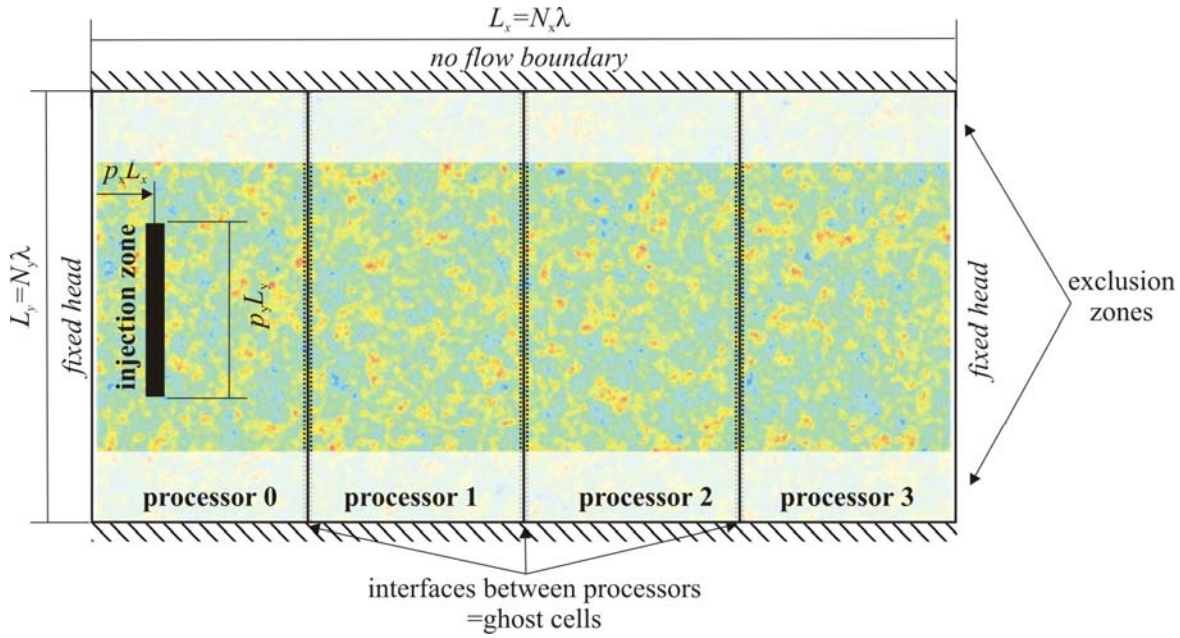

Figure 1: Permeability field stored on four processors, boundary conditions, injection and exclusion zones. The characteristics of the computational domain are $L_x=2048.l_m=204{,}8.\lambda$, $L_y=1024.l_m=102{,}4.\lambda$, $\lambda=10.l_m$ *and* $\sigma^2=2.25$ *where* λ *is the correlation length and* l_m *is the grid cell size. Permeability is increasing from blue to red. Computational domains used for asymptotic dispersion determination where 4 to 8 times longer and larger than this one.*

a)

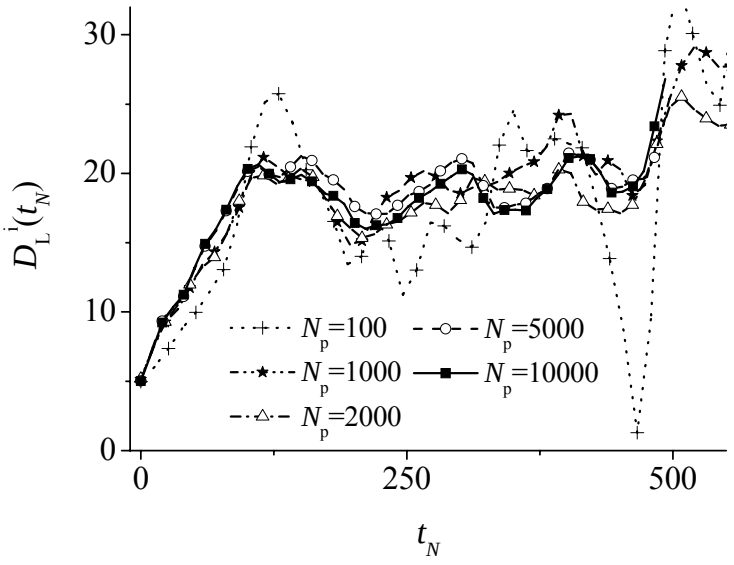

b)

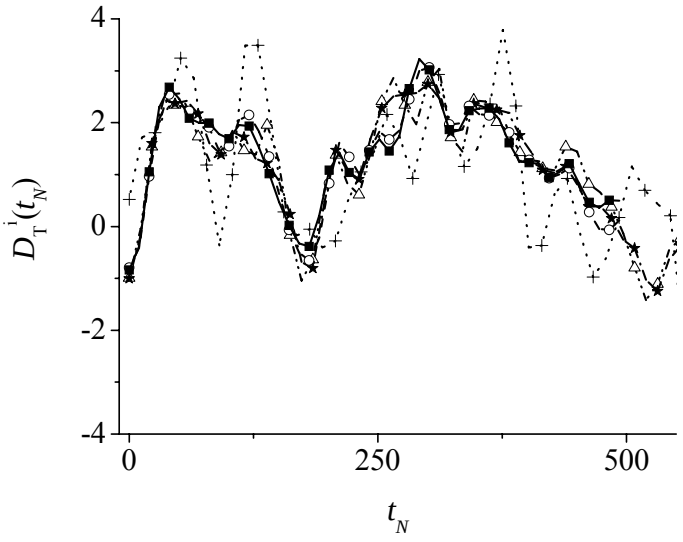

Figure 2 : a) Longitudinal and b) transverse dispersion coefficients as functions of time for increasing particle numbers with σ^2=9, λ=10 l_m and L_x=819,2.λ and L_y=819,2.λ (pure advection case).

a)

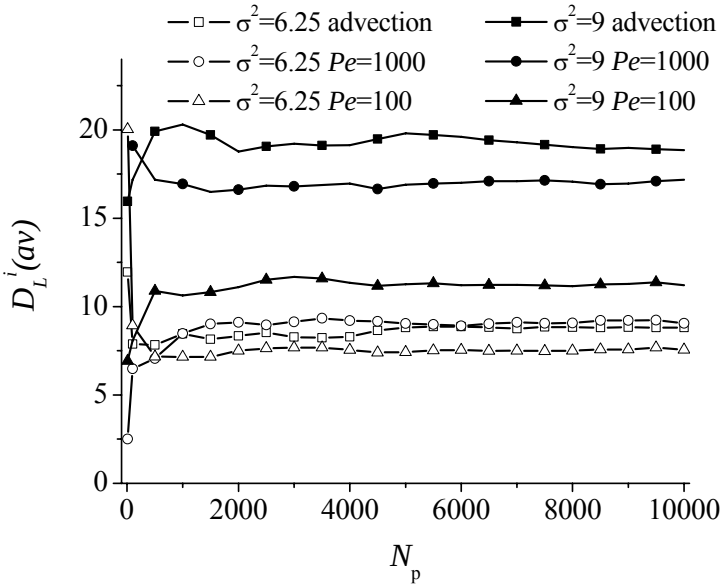

b)

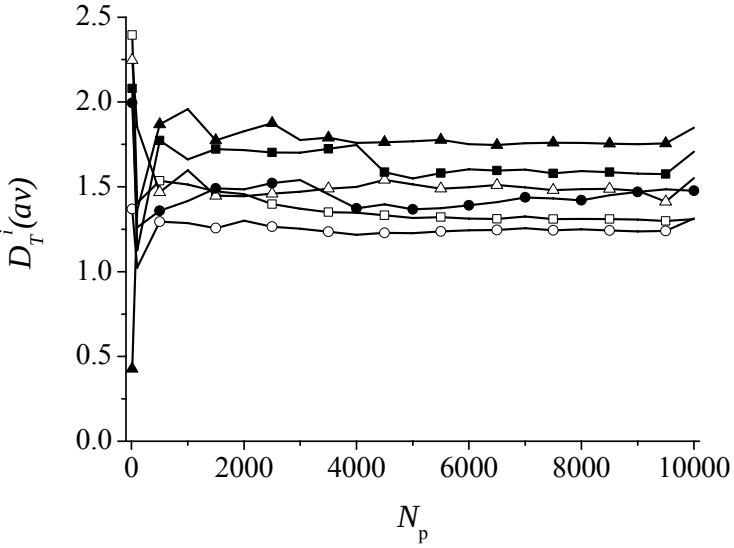

Figure 3: Asymptotic longitudinal (a) and transverse (b) dispersion coefficients as functions of the particle number N_p for L_x=1638,4 λ and L_y=819,2 λ. In this figure as well as in the following figures, the term advection in the legend refers to the pure advection case without diffusion and the legend is the same for both graphs.

a)

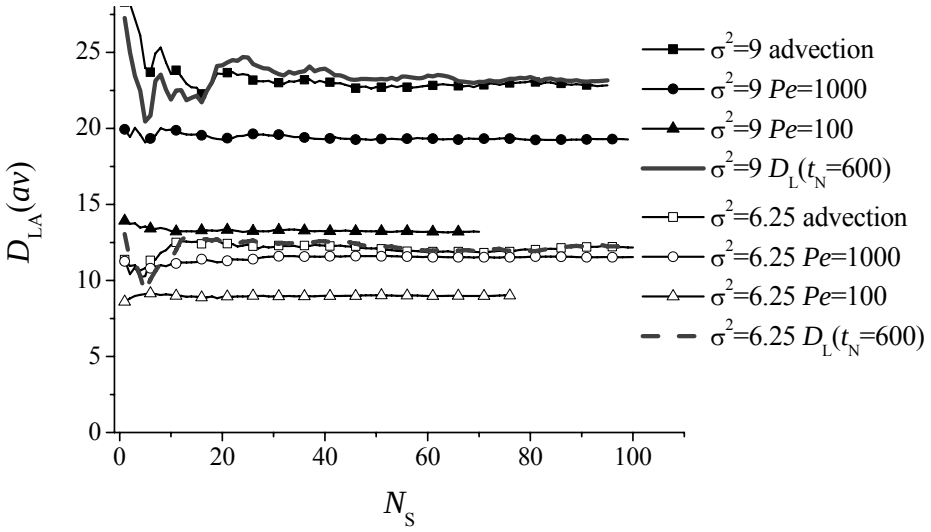

b)

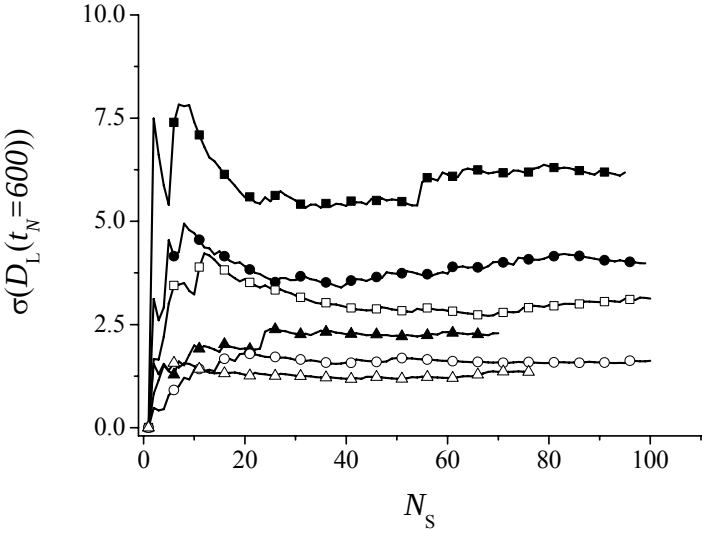

Figure 4: a) Asymptotic longitudinal dispersion coefficient and b) standard deviation of the dispersion coefficient at a given time t_N=600 as functions of the number of simulations for L_x=1638,4 λ and L_y=819,2 λ. In a), the dispersion coefficient D_L for t_N=600 has been added for the pure advection cases. t_N=600 is taken in the second half of the signal as the full signal length is around t_N=1000.

a)

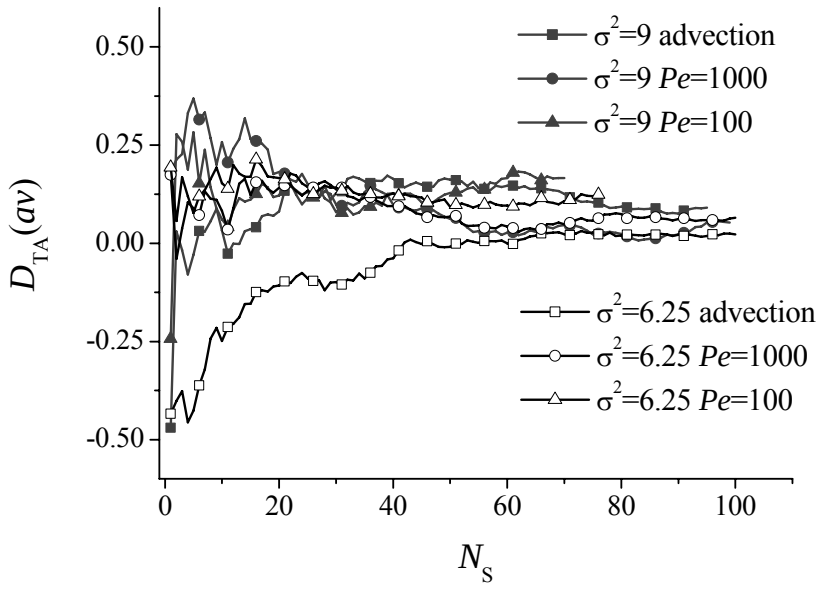

b)

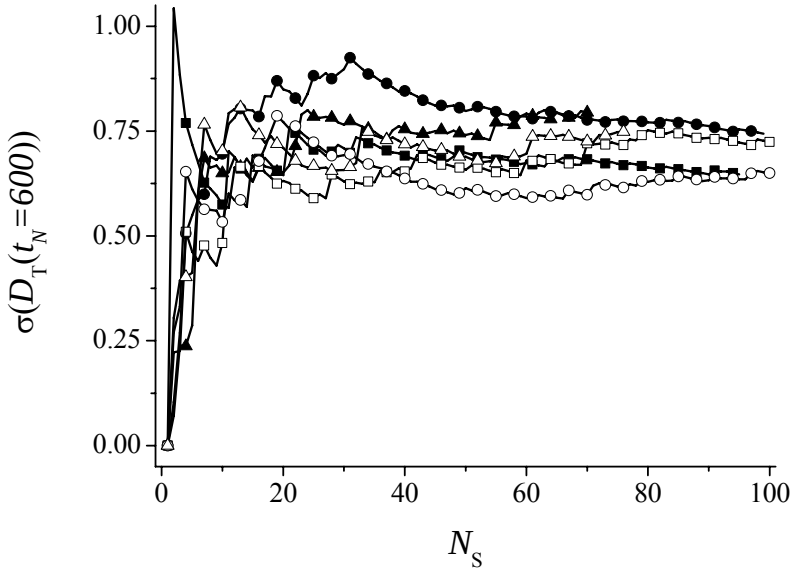

Figure 5: a) Asymptotic transverse dispersion coefficient and b) standard deviation of the dispersion coefficient at a given time t_N=600 as functions of the number of simulations. Same parameters as in figure 6.

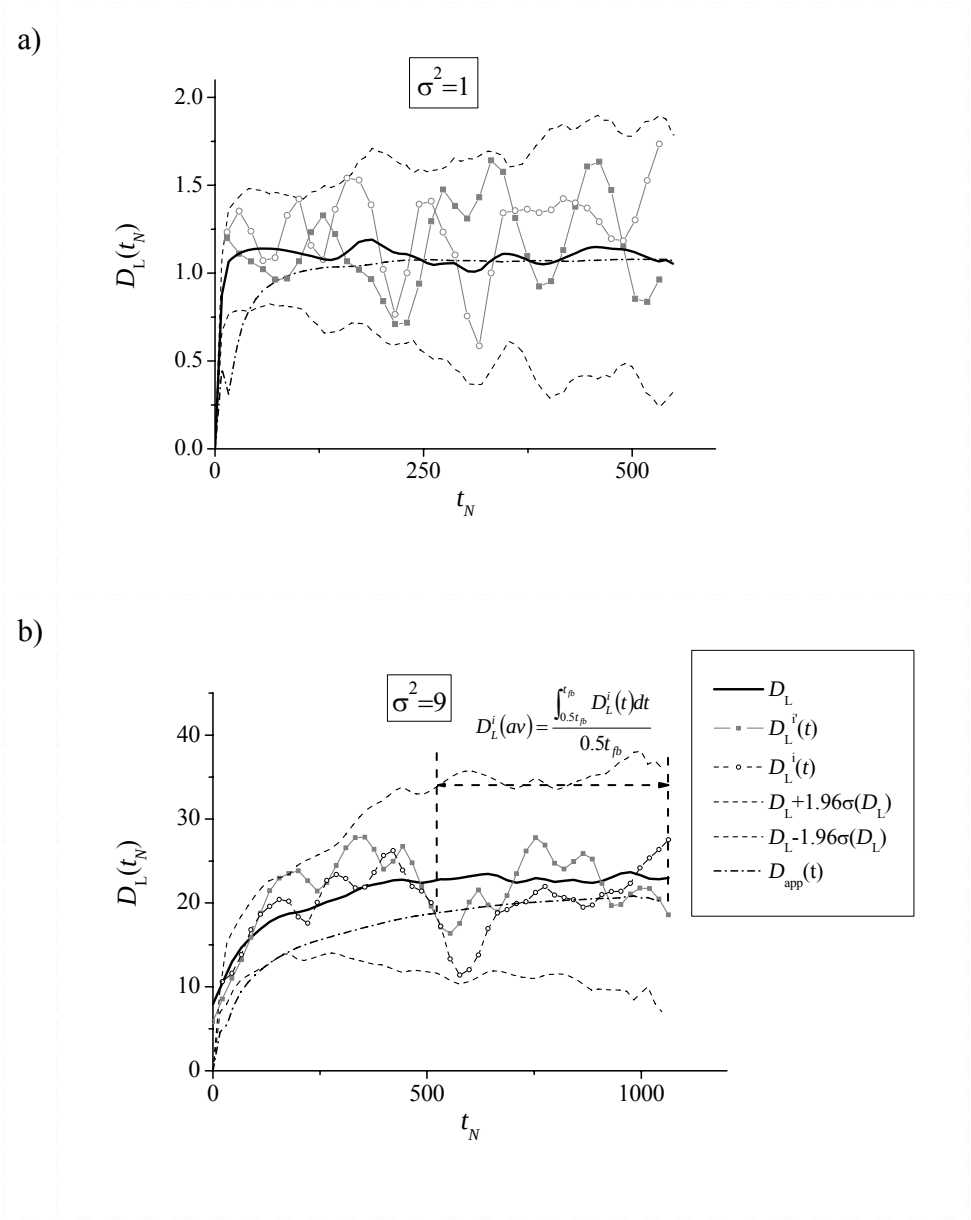

Figure 6: Normalized longitudinal dispersion coefficient for single realizations $D_L^i(t_N)$ *(points), their averages* $D_L(t_N)$ *over 100 realizations (lines) and the confidence interval at 95% on the dispersion coefficient (dashed line) (*σ^2*=1 and 9, pure advection case). The dashed-dotted line represents the normalized apparent dispersion coefficient* $D_{app}(t) = 0.5 < x^2(t) > / t$*. Computational domain size are for* σ^2*=1 (a)* L_x*=*L_y*=819,2* λ *and for* σ^2*=9 (b)* L_x*=1638,4* λ *and* L_y*=819,2* λ*.*

a)

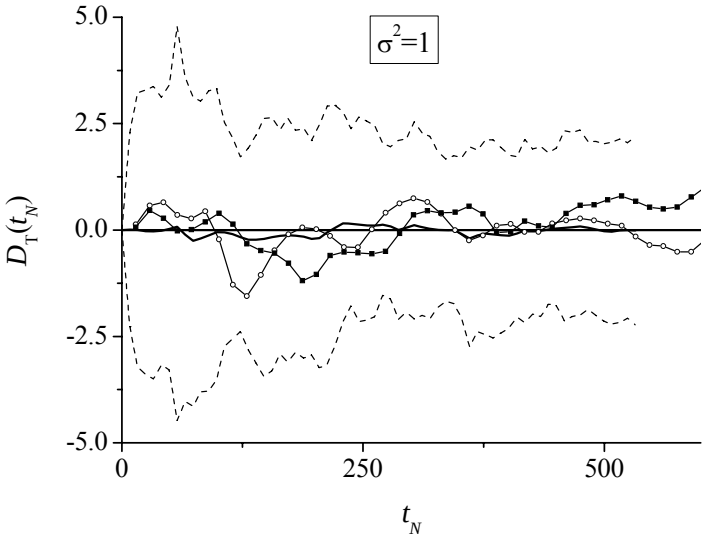

b)

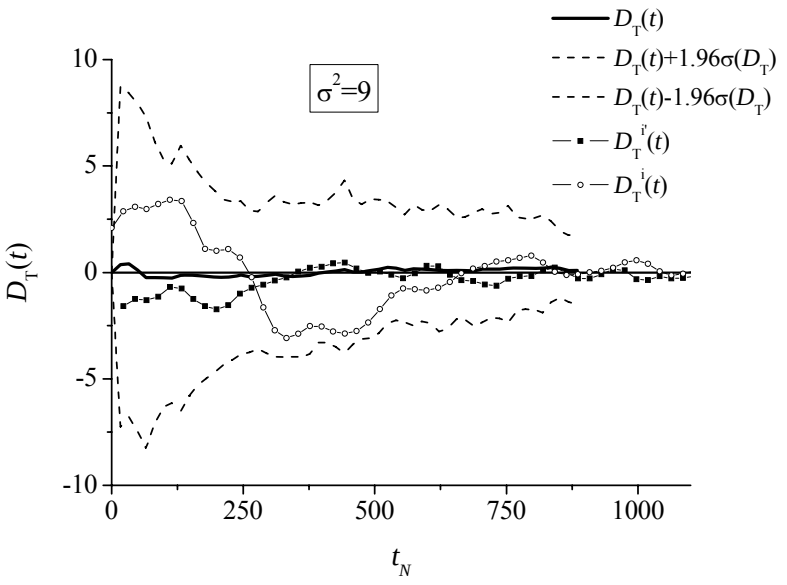

Figure 7: Normalized transverse dispersion coefficient. Same parameters as in figure 6.

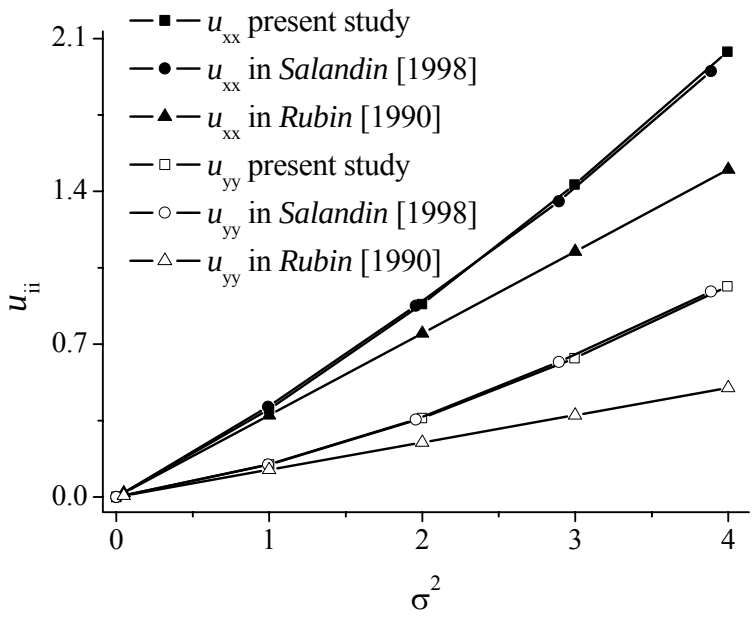

Figure 8: Velocity variance u_{xx} and u_{yy} as functions of σ^2 obtained analytically in Rubin [1990] and numerically in the present study and in Salandin and Fiorotto [1998].

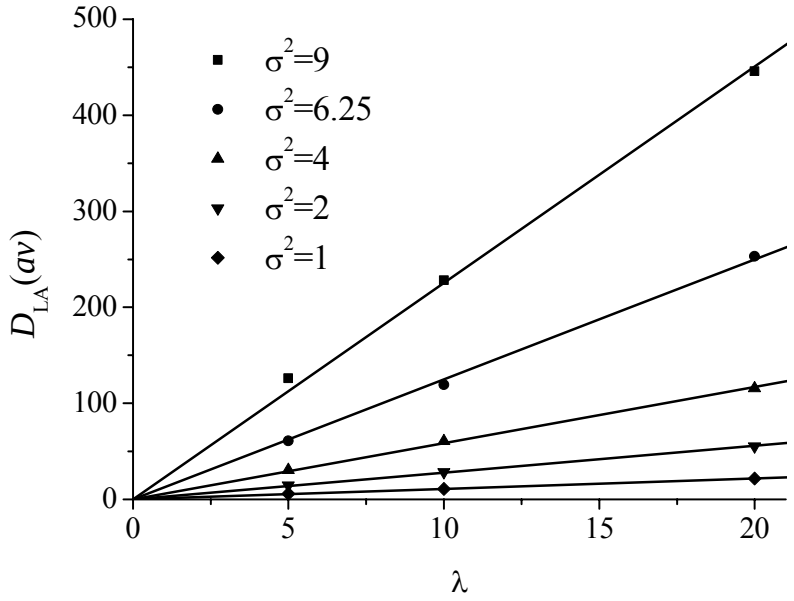

Figure 9 : Asymptotic longitudinal dispersion coefficient as a function of the correlation length for the pure advection case. Lines are linear fit through 0. Same parameters as in figure 6.

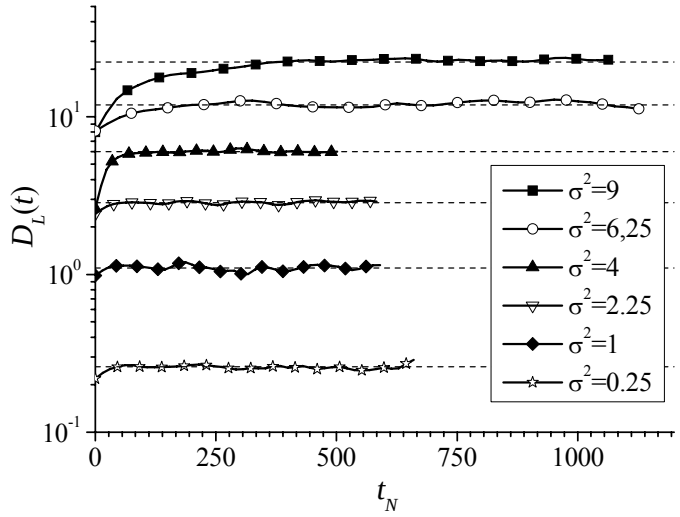

Figure 10: Longitudinal mean dispersion coefficient as a function of t_N for the pure advection case (time in terms of correlation scales crossed by the plume). Dashed lines mark the asymptotic coefficients. Same parameters as in figure 6.

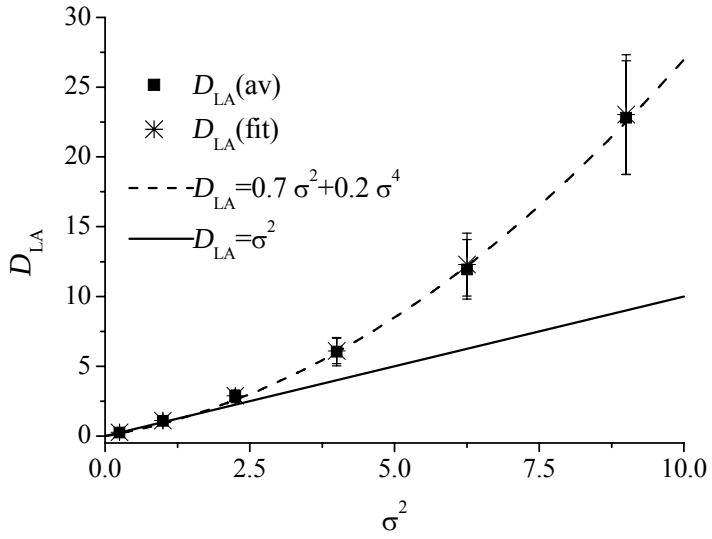

Figure 11: Normalized longitudinal asymptotic effective dispersion coefficient D_{LA} as a function of the variance of the log conductivity with pure advection. Vertical bars on data points represent the standard deviation on each side of the data point. D_{LA}(av) and D_{LA}(fit) are obtained respectively by averaging and fitting by an exponential function. Theoretical predictions [Gelhar, 1993] are represented by the line. The dashed curve stands for $0.7\sigma^2 + 0.2\sigma^4$. Same parameters as in figure 6.

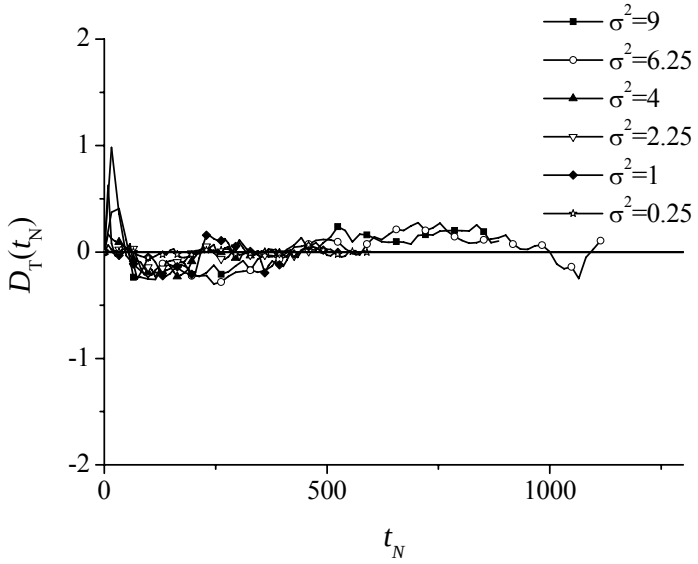

Figure 12 : Normalized transverse dispersion coefficient as a function of the normalized time in the pure advection case. Same parameters as in figure 6.

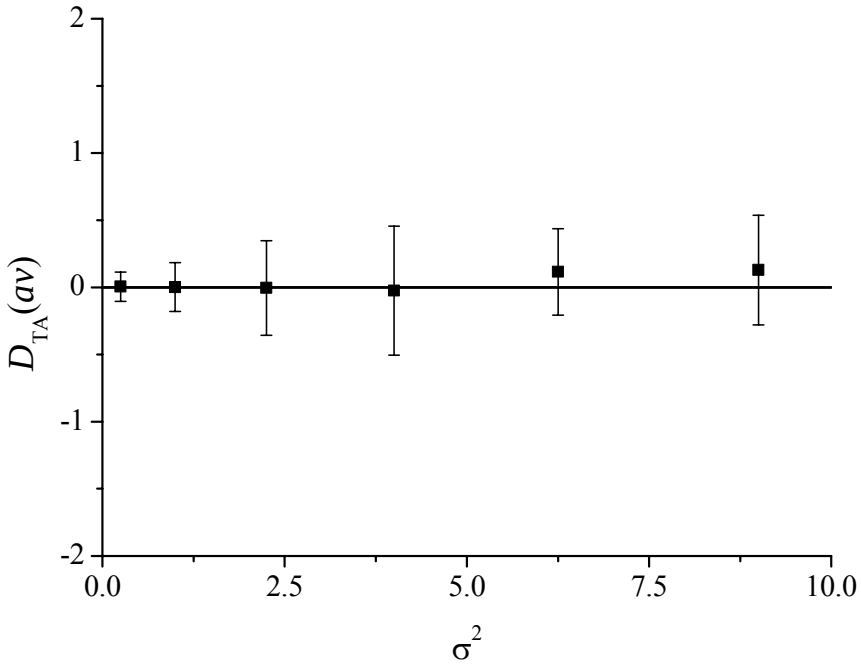

Figure 13 : Normalized transverse asymptotic dispersion coefficient for the pure advection case.

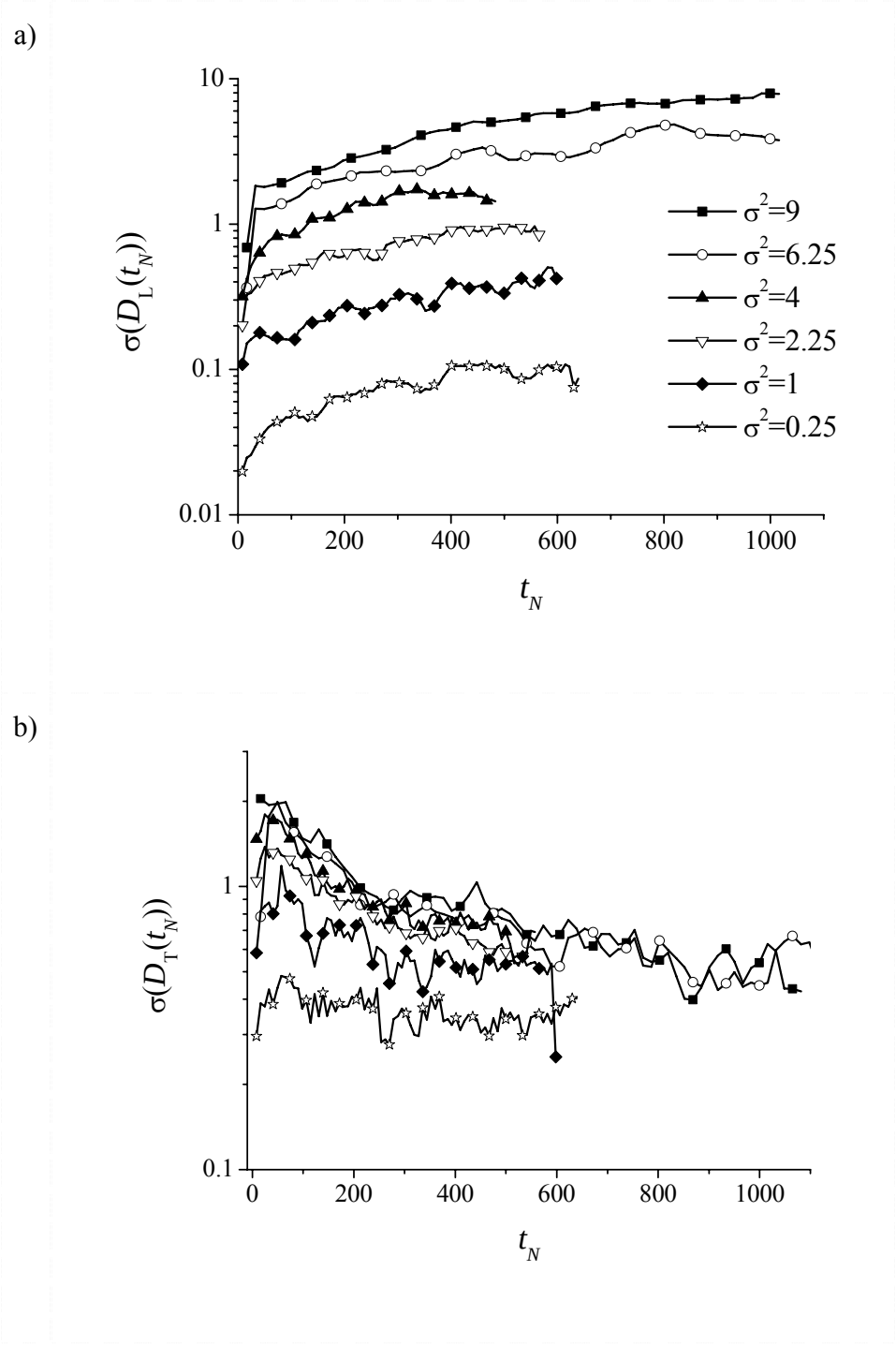

Figure 14 : Standard deviation of a) the longitudinal and b) transverse dispersion coefficients in the pure advection case.

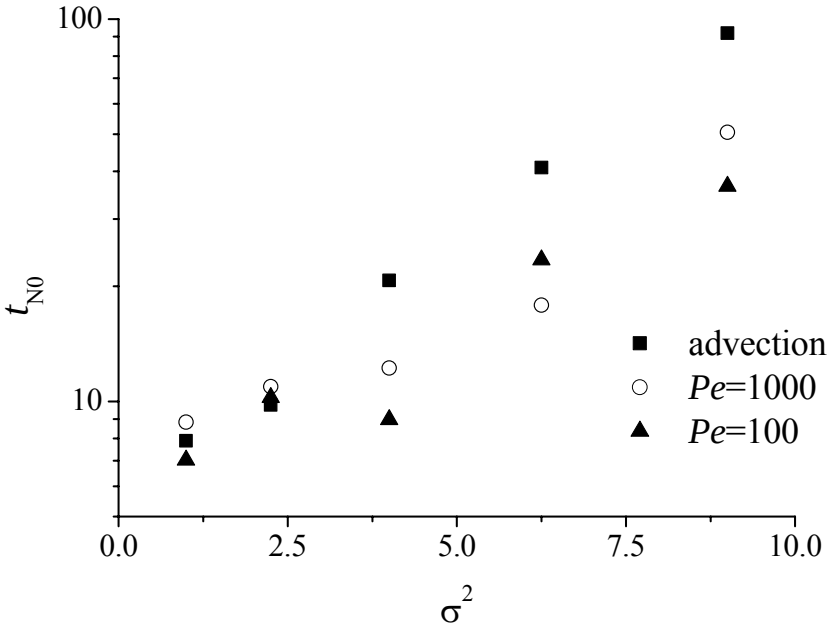

Figure 15 :Characteristic convergence time to the asymptotic regime t_{N0}.

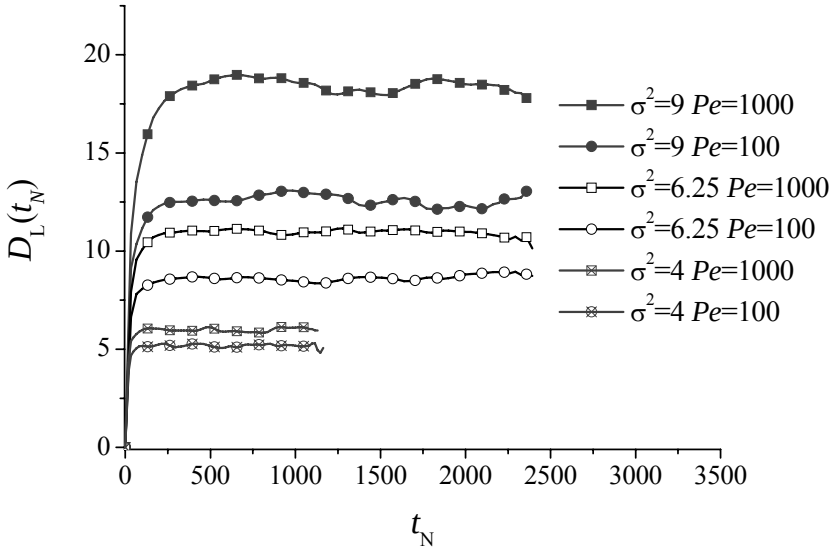

Figure 16: Longitudinal dispersion coefficient as a function of normalized time for $\sigma^2 \geq 4$.